THE NORTHERN LEVANTINE SEA CIRCULATION BASED ON COMBINED ANALYSES OF CTD AND ADCP DATA

Emin Özsoy and Hasan Güngör
Institute of Marine Sciences,
Middle East Technical University
P.K. 28 Erdemli, İçel, 33731 TURKEY

ABSTRACT

The circulation in the northern Levantine Sea is obtained from combined analyses of density distribution and current velocity data derived from CTD and acoustic Doppler current profiler (ADCP) measurements respectively. The method is based on multi-variate estimation, with artificial data inserted at the coasts to satisfy simplified boundary conditions.

Experiments have indicated sensitivity of the results to the relative weights and noise levels of the of independent sets of observations. Independent analyses of (*i*) frequently sampled ADCP data along the cruise track (*ii*) ADCP data at oceanographic stations, and (*iii*) CTD data at stations yielded results with varying degrees of success in resolving the small scales and in the realistic detection of eddies and jets, resulting in different levels of analysis error. The analysis of the combined CTD and ADCP data at stations yielded the best results. Coastal boundary conditions were successfully simulated by data insertion.

NATO ASI Series, Vol. I 19
Data Assimilation
Edited by P. P. Brasseur and J. C. J. Nihoul

INTRODUCTION

Recent observations in the Eastern Mediterrranean have revealed complex circulation features and an active dynamics with basin-wide excursions and interactions amongst current systems. Coherent eddies, persistent mid-basin and coastal current systems with meandering jets have been identified in the recent observations (Robinson *et al.*, 1991; The POEM Group, 1992; Özsoy *et al.*, 1989, 1991, 1993). Complexity of the regional circulation, as well as a lack of synoptic data in the past have deprived the region from being the subject of detailed investigations leading to a sound scientific understanding.

The Levantine and Ionian Seas are the two major basins of the Eastern Mediterranean, separated by the wide and relatively shallow waters of the Cretan Passage (Figure 1). The Levantine Sea is occupied by active dynamical structures with a wide range of scales (Özsoy *et al.*, 1989, 1991, 1993; Özsoy and Ünlüata, 1992, 1993). The Levantine Basin has been thoroughly covered by observations in the last 6-7 years. A mid-basin jet entering from the Cretan Passage and carrying modified Atlantic Water bifurcates into a number of smaller streams which circulate around permanent sub-basin scale gyres and eddies and contribute to the return flows along the coasts. The Levantine Sea is the source region of the Levantine Intermediate Water (LIW), created in the region as a result of winter time air-sea interactions. Seasonal and interannual variations are evident in the pattern of circulation. Every couple of years, the basin current systems drift between apparent circulation modes qualitatively linked with the intensity of LIW formation. Under extreme conditions, overturning is induced at the center of the permanent Rhodes Gyre, resulting in Deep Water formation, simultaneously with LIW formation (Sur *et al.*, 1992).

One of the outstanding features of the observed dynamical fields is the persistence of the coarse meso-scale to basin-scale coherent structures, which are relatively large compared to the Rossby radii of deformation ($L = 10 - 15\ km$ for the first baroclinic mode). However, superposed on this slowly evolving but swift system of currents, there is a rich signal in the meso-scale and sub-meso-scale features (Robinson *et al.*, 1987, The POEM Group, 1992; Özsoy, *et al.*, 1993).

In parallel with the improved observations, progress is being made in the modelling of Eastern Mediterranean circulation. General circulation models initialized with climatology and driven by atmospheric forcing are being used to approach realistic simulations

of the circulation consistent with model physics (*e.g.* Malanotte-Rizzoli and Bergamasco, 1989, 1991, Pinardi and Navarra, 1992; Zavatarelli and Mellor, 1992; Roussenov *et al.*, 1993). Dynamical process studies have used models with simplified physics to investigate the dynamics in sub-domains (*e.g.* Robinson *et al.*, 1991b; Robinson and Golnaraghi, 1992). Quasi-geostrophic ocean models, such as the full feature multi-level baroclinic model developed at Harvard University, including consistent boundary conditions applied at coastal boundaries (Milliff, 1990) and in multiply connected ocean domains (Özsoy *et al.*, 1992) are convenient for such studies.

In addition to the above circulation models, specific process models are also being used to explain the relationships between the atmospheric forcing, the circulation and the processes of water mass formation (*e.g.* Ovchinnikov and Plakhin, 1984; Brenner *et al.*, 1991; Feliks, 1991; Lascaratos *et al.*, 1993), or to explain eddy generation by instabilities of coastal currents (Feliks and Ghil, 1993).

There are also numerous recent attempts to calculate the seasonal or annual steady circulation of the Mediterranean consistent with climatological data and the physics of advanced circulation models (Tziperman and Malanotte-Rizzoli, 1991; Roussenov *et al.*, 1992; Bergamasco *et al.*, 1993; Brasseur *et al.*, 1993), employing various types of data assimilation and inverse techniques. Alternatively, the time dependent circulation is computed from quasi-synoptic data (Bergamasco, 1993), by making use of adjoint data assimilation techniques.

Our objective in the following is to improve the estimation of synthesized fields from observations, and initialize a quasi-geostrophic ocean model with these fields. With the recent addition of a vessel mounted ADCP system, the R/V BİLİM of the IMS-METU has increased its data collection capacity, and we therefore test analysis schemes to determine how much use can be made of this increased data coverage, especially under conditions of uneven and mixed data distribution. In estimating the initial fields, we utilize independent measurements of the density field obtained by a CTD profiler, and current measurements obtained by the ADCP system. A multi-variate method is used to analyse the data, satisfying boundary conditions at coastal and island boundaries. We also make tests to ensure that the resulting boundary values are consistent with the dynamical modes of the model.

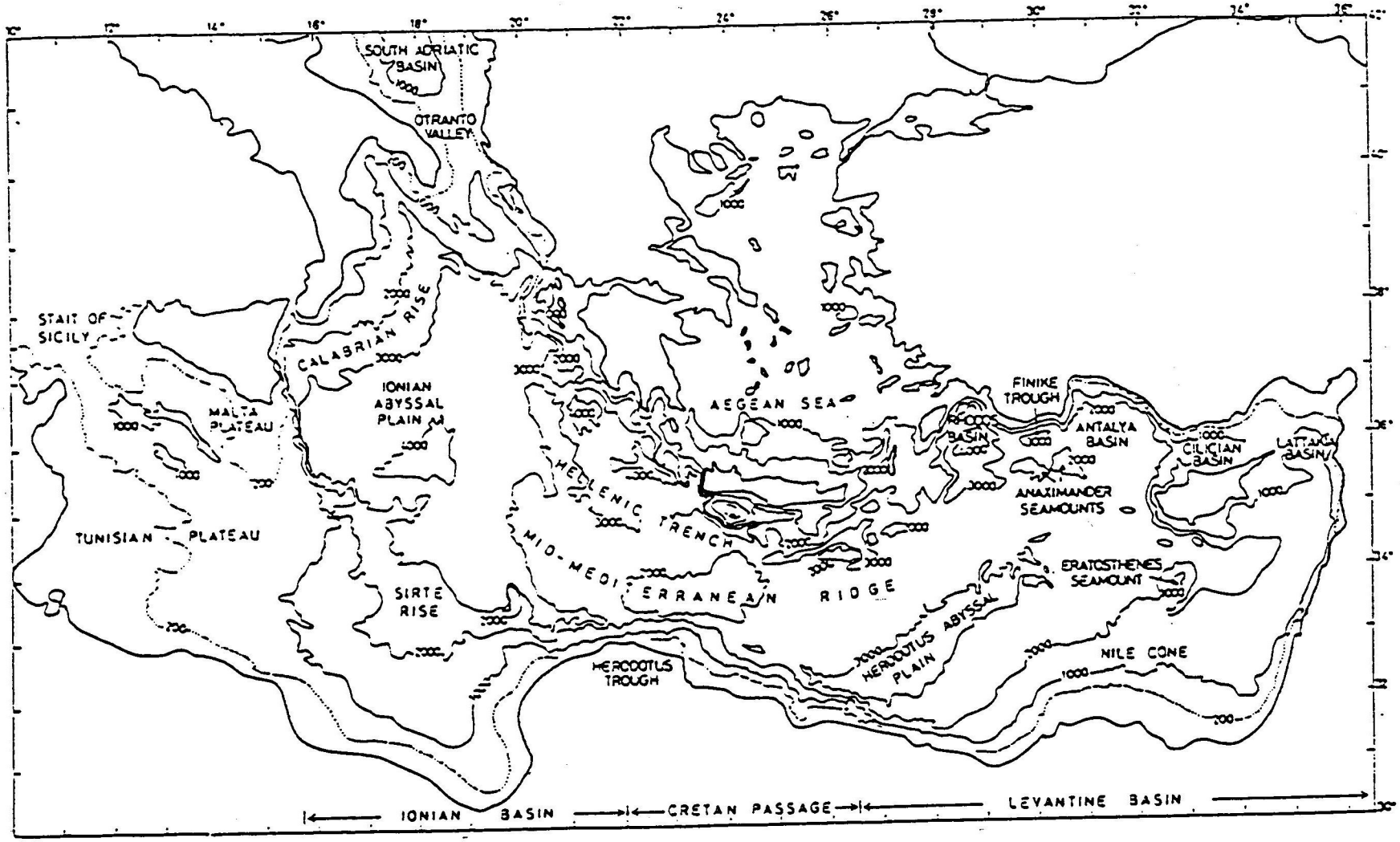

Figure 1 Location map and bathymetry of the Eastern Mediterranean, including the Levantine Basin.

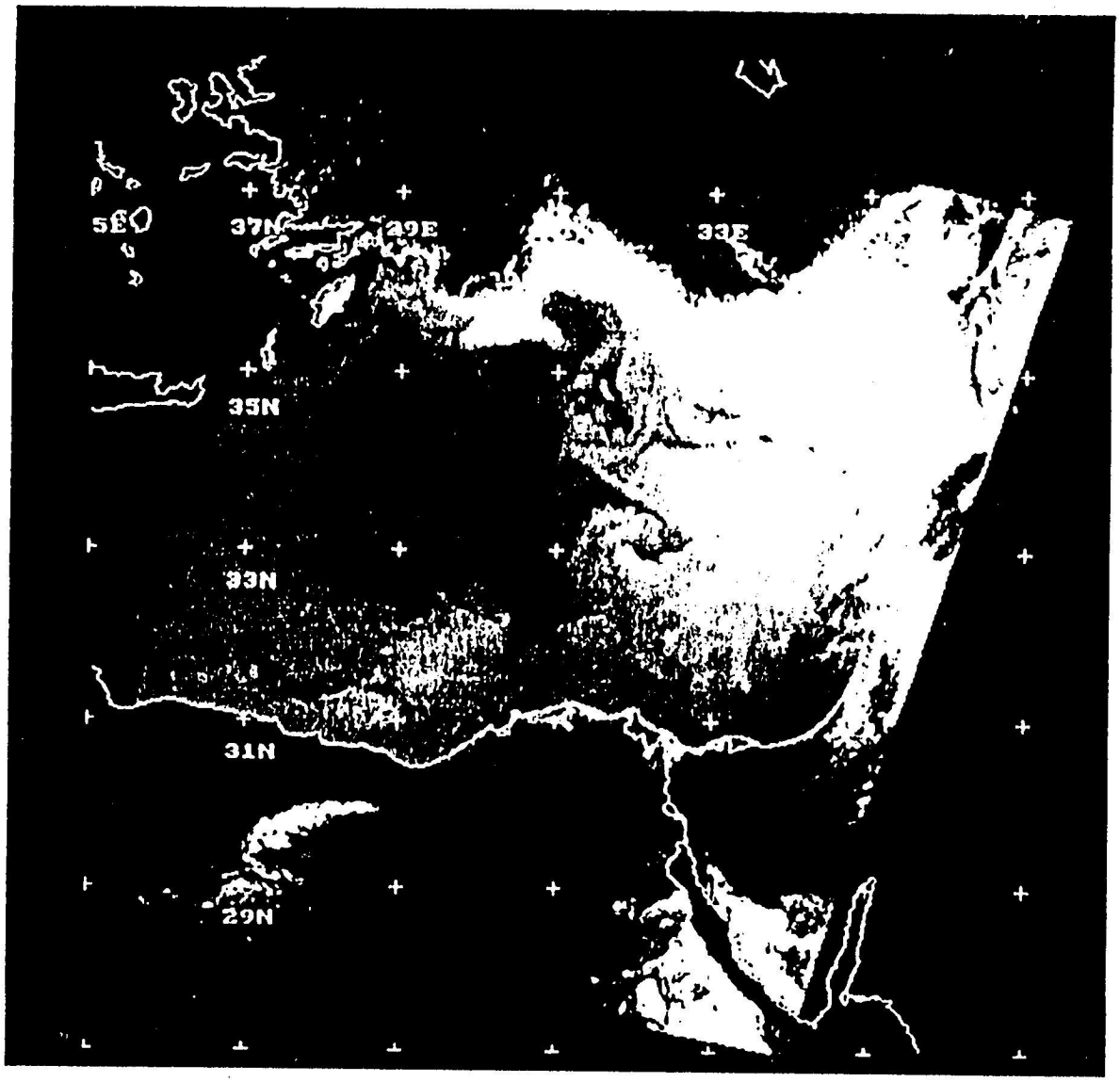

Figure 2 AVHRR satellite image of the Levantine Basin on 24 September 1991, NOAA-10

A DESCRIPTION OF THE CIRCULATION

We use the observations made during October 1991 in the northern Levantine Sea. The surface temperature expressions obtained from an AVHRR satellite image during the same period (Figure 2) shows the cyclonic Rhodes Gyre (the dark/cool region covering a large part of the basin in the west), encircled by current systems and eddies. The warm region to the south of the basin is the dispersion region of the currents entering the basin from the west, embodying many anticyclonic eddies. Of these, the uniform circular eddy southeast of Crete is a semi-permanent feature which has consistently been observed in the same location in the repeated surveys of 1987, 1989, 1990 and 1991 (Robinson *et al.*, 1991, Özsoy *et al.*, 1993). Another anticyclonic eddy is connected to the Southeast Cretan Eddy by a filament and extends east towards the interior of the Rhodes Gyre circulation. Other eddies are found along the Egyptian coast. The intense warm spot south of Cyprus corresponds to the Shikmona Eddy, a permanent feature of the Levantine Sea circulation (Robinson *et al.*, 1991, Özsoy *et al.*, 1993). A cyclonic region is observed immediately northeast of the Shikmona eddy. The warm region north of Cyprus and along the Turkish coast is the Asia Minor Current, a meandering but permanent feature of the circulation. It can be noted that the Rhodes Gyre circulation is limited to the area between the islands of Crete and Cyprus in this case, with its peripheral currents largely bypassing west of Cyprus and not extending further east as it was observed in some earlier cases (Özsoy *et al.*, 1993). The Rhodes Gyre peripheral currents head north near western Cyprus and reinforce the Asia Minor Current along the west coast of Anatolia.

THE DATA

The oceanographic data collected by the R/V BİLİM of the IMS-METU in the northern Levantine Sea during October 1991 included CTD station data for temperature and salinity, and acoustic Doppler current profiler (ADCP) measurements obtained at oceanographic stations and along the ship's track.

The salinity and temperature data were collected by a Seabird Model 9/11 CTD profiler system at 71 oceanographic stations nominally spaced at half degree intervals in the norhern Levantine Sea. The vertical resolution of the data is $1m$ after bin averaging. Dynamical height anomaly was computed from the density data, relative to a reference level of $1000m$. The analysis of surface streamfunction, based on hydrographic data is

shown in Figure 3a. It can be verified that the circulation has much in common with the AVHRR satellite data shown in Figure 2.

The current measurements were obtained using an RD Instruments ADCP system with a vessel-mounted $150Khz$ transducer. A bin size of $2m$ was used in the data collection, and up to 128 depth bins were sampled, starting from below the ship keel. Ensemble averaging was carried out at half hour intervals at oceanographic stations. Under cruising conditions, the data were ensemble averaged with 10 minute intervals. The data obtained under way yielded current velocity profiles at about 1200 positions along the entire cruise track. The ensemble averaging interval of $10min$ is marginally good to obtain reliable data during cruising. Due to limitations of acoustic penetration, reliable measurements (90% percent good) were obtained only for depths smaller than $200 - 250m$.

Although GPS navigation was available and position data were collected, they were not used to compute absolute velocity because of insufficient accuracy and noise problems. Absolute velocity was computed by adjusting the velocity profile relative to the average of the measured currents in a reference layer between $160m$ and $200m$ depths. Although we did not have independent measurements to confirm the absolute currents, we used geostrophic currents derived from the density field (Figure 3b) to check that the ADCP reference layer velocities were indeed small. In fact, we added these derived reference velocity values to the ADCP reference layer velocity, and could not observe noticable differences in the final fields. The ADCP current measurements obtained at $20m$ depth along the cruise track during of R/V BİLİM are shown in Figure 3c.

METHODOLOGY

The integration of available observations into valid initial fields of dynamical variables is a necessary first step in the initialization of a model. The methodology of objective analysis is widely used for this purpose, and has been applied to oceanographic fields by Bretherton *et al.* (1976), who developed it for both scalar and vector fields. McWilliams *et al.* (1986) further developed the methodology to be applied to multivariate analyses and to the analyses of derived fields based on physical laws. Carter and Robinson (1987) made improved vector analyses of the velocity field. Robinson and Leslie (1985) combined statistical and dynamical models to make improved and consistent estimates of initial physical fields.

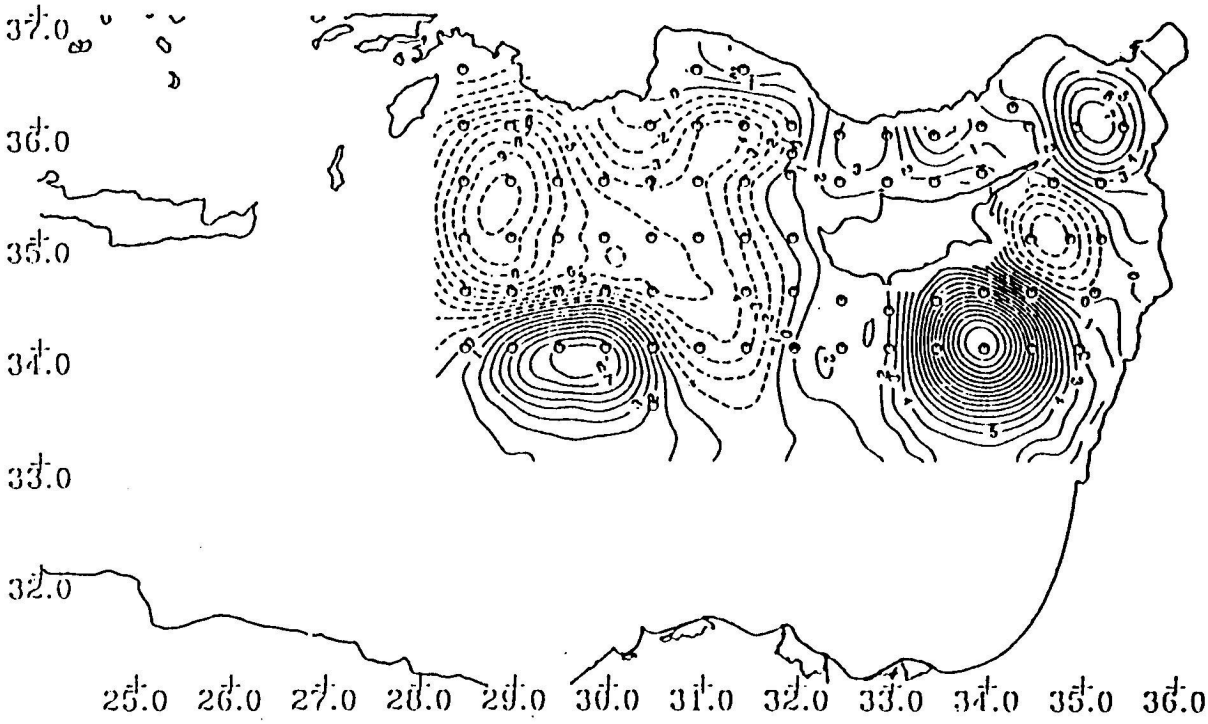

Figure 3.(a) Dynamic height anomaly (cm) at 20 m depth computed from CTD data, referenced to a 1000 decibar level of no motion, October 1991..

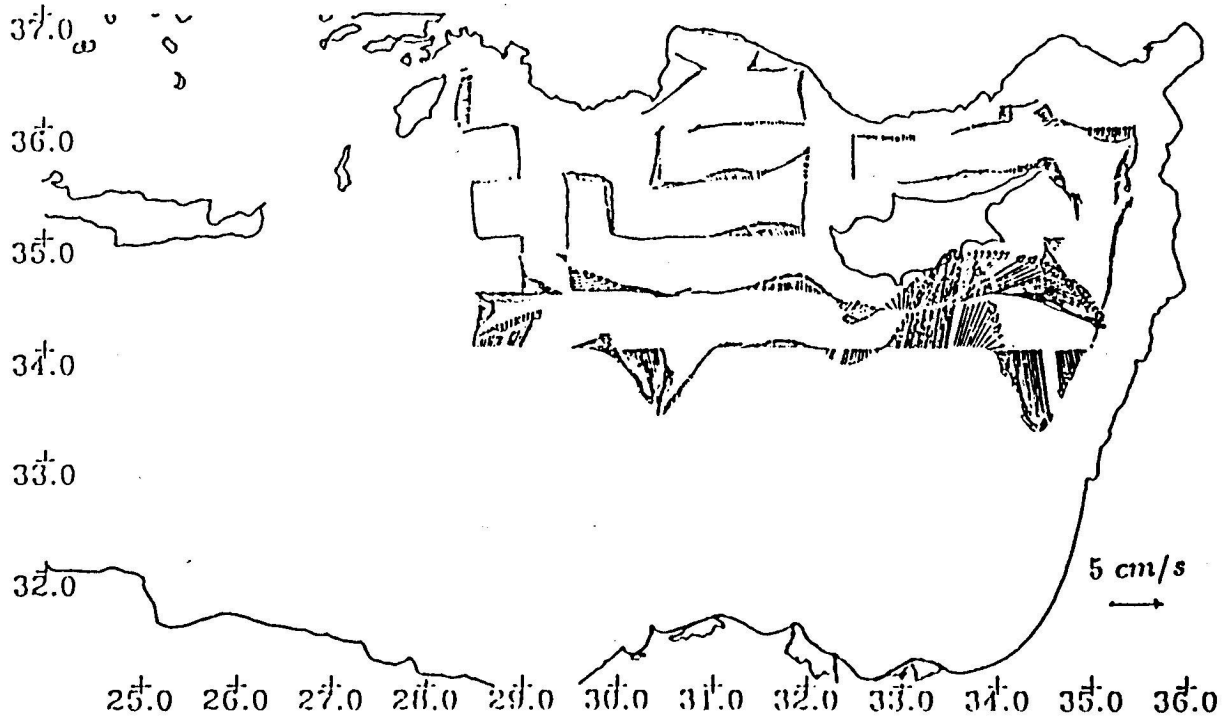

Figure 3.(b) Currents at 200 m depth derived from the dynamic height anomaly data and projected on the cruise track by objective analysis.

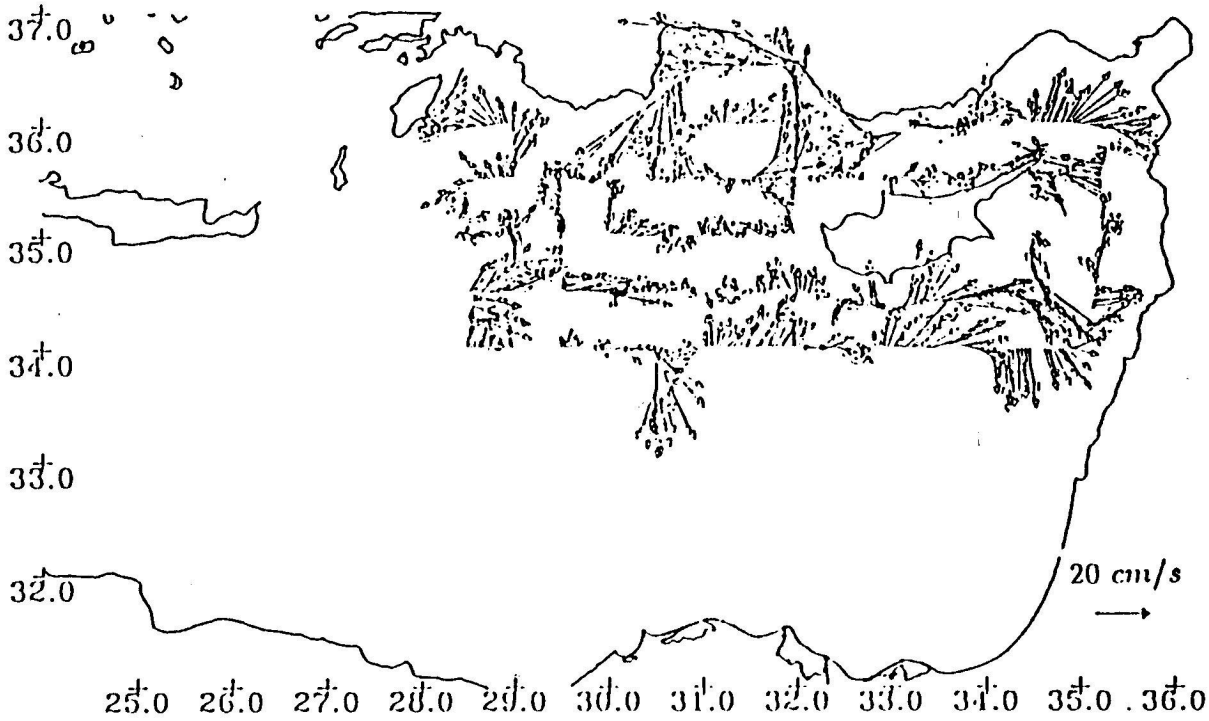

Figure 3.(c) ADCP current velocity ensemble averaged every 10 min interval along the cruise track, and adjusted by adding the 200 m velocity field in (b).

Although the ADCP is a modern instrument which has found widespread use in oceanography, the large volume of data it can generate is often not immediately available for interpretation, *e.g.* for the determination of synoptic or time-dependent oceanographic fields. The measurements are often biased by transience resulting from inertial, internal and tidal fluctuations, and extraneous noise. Reliability is gained by averaging of data obtained at fixed position *i.e.* at an oceanographic station. For ADCP data collected while the ship is under way, time averaging is compromised against unwanted spatial averaging. Observational errors are increased considerably as a result of ship motions, especially in rough seas (Saunders, 1992).

Combined analyses of ADCP and CTD data for improved dynamical field estimates are rare in oceanography. More commonly, the data are patched together and compared with other sets of observations for a better description of circulation (*e.g.* Saunders, 1992). On the other hand, some earlier studies only used ADCP station data, without attempting to use the full data sets. Walstad *et al.* (1991) have computed the reference velocity field from ADCP current velocity measurements at stations, and have added to this the dynamic height computations to obtain fields consistent with dynamics.

The streamfunction obtained from dynamic height is generally smooth because it is obtained by integrating density using a geostrophic relationship. In addition, it represents a non-divergent velocity field by definition. On the other hand, the measured velocity field can both be noisy and divergent. Although it is possible to obtain both the non-divergent and the irrotational velocity components from current velocity measurements (Robinson and Carter, 1987), it is often the non-divergent part that we are generally interested in, especially in the case of numerical models. Robinson and Carter (1987) determine the non-divergent streamfunction by solving an inverse problem, with current observations analysed first to form a regular grid of velocity data. An alternative approach proposed by Bretherton *et al.* (1976) and McWilliams *et al.* (1986) is to use a correlation model satisfying a non-divergent relationship between pressure and velocity.

The analysis scheme

We use multivariate statistics with a non-divergent correlation model to estimate dynamical fields from unevenly distributed, large sets of mixed data. Observations of dynamical height anomaly ψ obtained from CTD data and ADCP velocity components u, v are used after normalizing each variable by the corresponding sample standard deviation, namely σ_ψ, σ_u and σ_v. We estimate a variable, θ, at an analysis point $\vec{x} = (x, y)$, from a linear combination of available observations of ψ_p at CTD stations $\vec{x}_p = (x_p, y_p)$, $p = 1, \ldots P$, and ADCP velocity measurements $\vec{u}_q = (u_q, v_q)$ at points $\vec{x}_q = (x_q, y_q)$, $q = 1, \ldots Q$:

$$\left(\frac{\theta_r}{\sigma_\theta}\right) = \sum_p \alpha_{rp}\left(\frac{\psi_p}{\sigma_\psi}\right) + \sum_q \alpha_{rq}\left(\frac{u_q}{\sigma_u}\right) + \sum_q \alpha_{rq}\left(\frac{v_q}{\sigma_v}\right) \qquad (1)$$

The analysis variable θ stands for either ψ, u, or v; since normalization is introduced, the analysis scheme is the same for any one of the variables. For simplicity, we change the notation to represent already normalized variables, and discontinue differentiating between observation types to write

$$\theta_r = \sum_{s=1}^{N} \alpha_{rs}\phi_s, \qquad (2)$$

understanding that $\{\phi\}$ is the array of mixed, normalized observations of length $N = P + 2Q$, and $\{\alpha\}$ is the nondimensional coefficient array of equal length.

Note that the observations contain measurement errors and noise which make them different from true values Φ_s by some small amount: $\phi_s = \Phi_s \pm \epsilon_s$. Similarly, we expect that the analysis involves estimation errors relative to the true values: $\theta_r = \Theta_r \pm s_r$. The estimation error variance over an ensemble of analysis points $\vec{r}_k$, $k = 1, \ldots M$ is

$$\langle s_r^2 \rangle = \langle (\theta_k - \Theta_k)^2 \rangle = \langle \sum_s a_{ks} \phi_s \rangle. \tag{3}$$

Mininizing this variance with respect to the choice of a yields

$$a_{ks} \langle \phi_s \phi_l \rangle = \langle \Theta_k \phi_l \rangle. \tag{4}$$

In the above, angled brackets imply ensemble averages. The coefficients a in equation (4) are determined from statistical correlation functions. These are respectively the autocorrelation of the observations and the cross-correlation of true values versus the observations, simplified as

$$A_{sl} \equiv \langle \phi_s \phi_l \rangle = \langle \Phi_s \Phi_l \rangle + \langle \epsilon_s \epsilon_l \rangle \equiv \hat{C}_{sl} + E\delta_{sl}$$
$$C_{kl} \equiv \langle \Theta_k \phi_l \rangle = \langle \Theta_k \Phi_l \rangle.$$

Note that the matrix of correlations C is a subset of $\hat{C}$, because it only includes the correlations of the analysed variable Θ with the complete set of measured variables Φ (its dimensions are either $P \times N$ or $Q \times N$ depending on the variable being analysed), while $\hat{C}$ includes correlations of the complete set of variables (dimension $N \times N$). It is also assumed that no correlations exist between true values and observations, and between observation errors for independent measurements. Further, the standard error variance of the measurements is assumed to have a constant value of E applied to all measurements. The entries of the correlation matrices A and C are evaluated for each data pair, based on a correlation model such as the one we present in the following.

The analysis and its variance are then obtained as

$$\theta_r = \sum_{r=1}^{N} C_{rr} \sum_{s=1}^{N} A_{rs}^{-1} \phi_s,$$
$$\langle s_r^2 \rangle = C_{rr} - \sum_{r=1}^{N} \sum_{s=1}^{N} C_{rr} C_{rs} A_{rs}^{-1}.$$

The correlation model

Because ensemble statistics are usually not available, the correlation function is replaced by a model. For simplicity, we assume statistical homogeneity and isotropy, and leave only few free parameters in the model to be determined by comparison with the observed data. The model for the spatial correlation of the dynamic height anomaly (ψ) is selected to be

$$F_{\psi\psi} = \{1 \pm (R/A_2)^2 \pm (R/A_3)^3 \ldots \pm (R/A_n)^n\} e^{-\frac{1}{2}(\frac{R}{B})^2} \tag{5}$$

where $R = \sqrt{(\Delta x)^2 + (\Delta y)^2}$, Δx and Δy are the x and y distances between pairs of observations, and A_1 to A_n and B are dimensional scales.

The above is an extension of earlier models appearing in the literature (*e.g.* Bretherton *et al.*, 1976; Robinson *et al.*, 1991) to include more than the first two terms. To ensure positive definiteness of the correlation matrix (real valued wave-number spectrum of a scalar as shown by Bretherton *et al.*, 1976; Denman and Freeland, 1985), we leave out the term proportional to the first power of the distance, *i.e.* the only assymetric term yielding a gradient at $R = 0$.

The streamfunction obtained from the mass field (the dynamic height anomaly) involves assumptions of small vertical velocities and geostrophy, which constrain the velocity field to be non-divergent:

$$\vec{u} = \hat{k} \times \nabla\psi. \tag{6}$$

The complete set of correlation functions, consistent with the above relation are therefore obtained as:

$$\begin{aligned}
F_{\psi\psi} &= \{1 + a_2 r^2 + a_3 r^3 + \ldots a_n r^n\} e^{-r^2/2} \\
&= \{1 + \sum_{k=2}^{n} a_k r^k\} e^{-r^2/2} \\
F_{uu} &= \frac{1}{(1-a_2)} \left\{ \left(\frac{x}{r}\right)^2 (\rho - \sigma) + \sigma \right\} \\
F_{vv} &= \frac{1}{(1-a_2)} \left\{ \left(\frac{y}{r}\right)^2 (\rho - \sigma) + \sigma \right\} \qquad (7a-f) \\
F_{uv} &= \frac{1}{(1-a_2)} \left(\frac{xy}{r^2}\right) (\rho - \sigma) \\
F_{u\psi} &= \frac{1}{\sqrt{1-a_2}}\, y\rho \\
F_{v\psi} &= -\frac{1}{\sqrt{1-a_2}}\, x\rho
\end{aligned}$$

where

$$\rho(r) = -\frac{1}{r}\frac{dF_{\psi\psi}}{dr} = \{1 + \sum_{k=2}^{n} a_k(r^2 - k)r^{k-2}\}e^{-r^2/2}$$

$$\sigma(r) = -\frac{d^2F_{\psi\psi}}{dr^2} = \{(1 - r^2) + \sum_{k=2}^{n} a_k\{-r^4 + (2k+1)r^2 - k(k-1)\}r^{k-2}\}e^{-r^2/2} \quad (8a, b)$$

and a_k are dimensionless polynomial coefficients:

$$a_k = \pm(B/A_k)^k.$$

Distance is normalized with respect to the decay scale B, such that $x = \Delta x/B$, $y = \Delta y/B$, and $r = R/B = \sqrt{x^2 + y^2}$. Because correlation functions are already divided by standard deviations of the corresponding variables, a factor proportional to $1 - a_2$ results in the denominator.

Determination of model coefficients

In principle, it is possible to find the coefficients A_k and B to yield best agreement between model and observed correlations. We seek to find them by least squares method, comparing the experimental correlations $C_{\chi_i\chi_j}$ (calculated from the data) with model correlations $F_{\chi_i\chi_j}$, *i.e.*

$$\langle\Sigma\epsilon^2\rangle = \sum_{i,j}\langle(C_{\chi_i\chi_j} - F_{\chi_i\chi_j})^2\rangle$$

where the angled brackets represent averages of data pairs, and the terms in the summation include the set of possible correlation functions between variables $\{\chi\} = \{\psi, u, v\}$. Because the model correlation functions are not linear in the coefficients, *i.e.* they involve the yet undetermined coefficient a_2 in the denominator and the decay scale B in the normalizations, the least squares procedure requires a double iteration to determine a_k, first by varying B, then for fixed values of B varying a_2 until best agreement is found.

The experimental correlation functions $C_{\chi_i\chi_j}$ (averages computed per 20 km square) derived from the data of Figures 3a and 3c are shown in Figure 4. Note that the u and v velocity components have decorrelation scales of less than 100 km, while the dynamic height anomaly ψ statistics is anisotropic, with scales of $\sim$ 100 and 200 km in the principal directions.

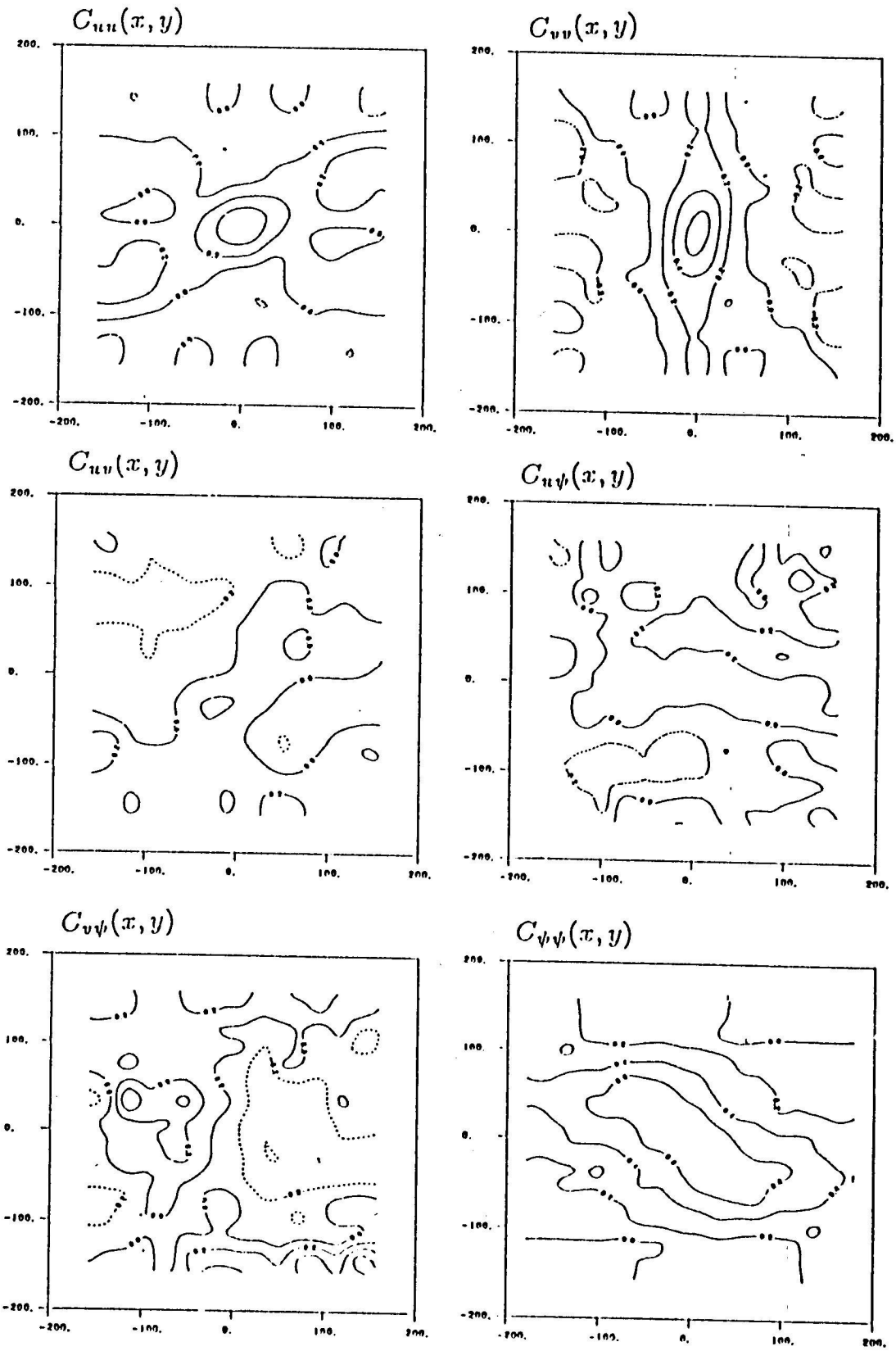

Figure 4.(a-f) Experimental correlation functions computed from the ψ, u and v data. Statistical averages within 20 km squares are plotted.

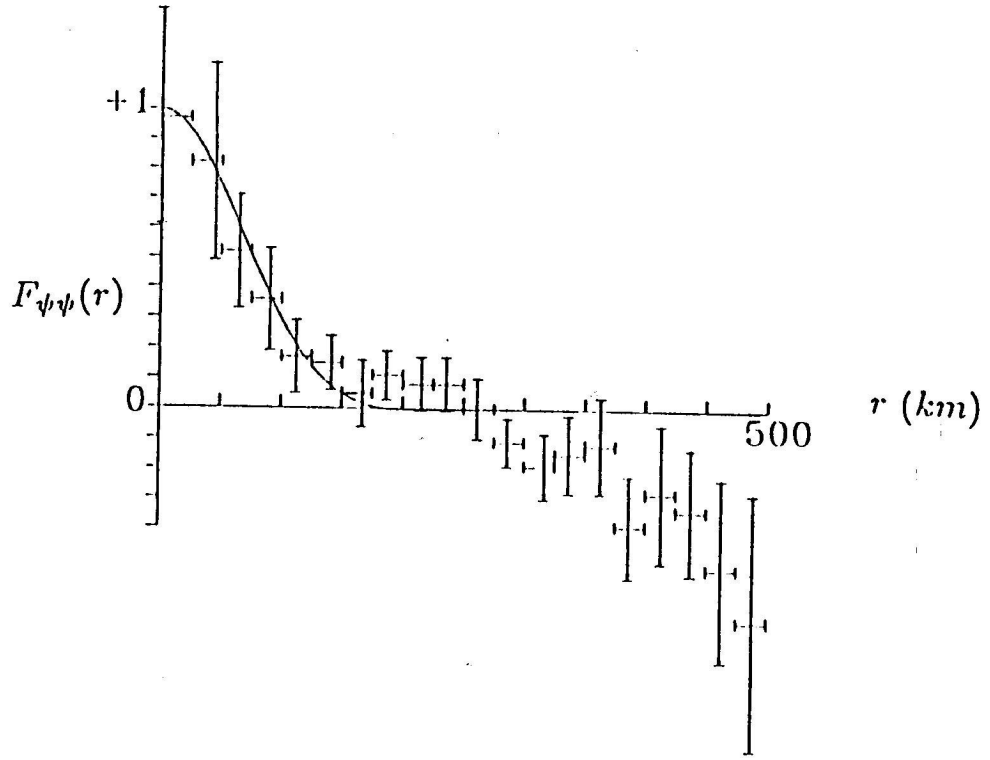

Figure 5.(a) Comparison of experimental and model correlations for a two term representation of (7a). The experimental correlations are averaged every 25 km (horizontal bars), and the 95 % confidence limits are indicated by vertical bars,

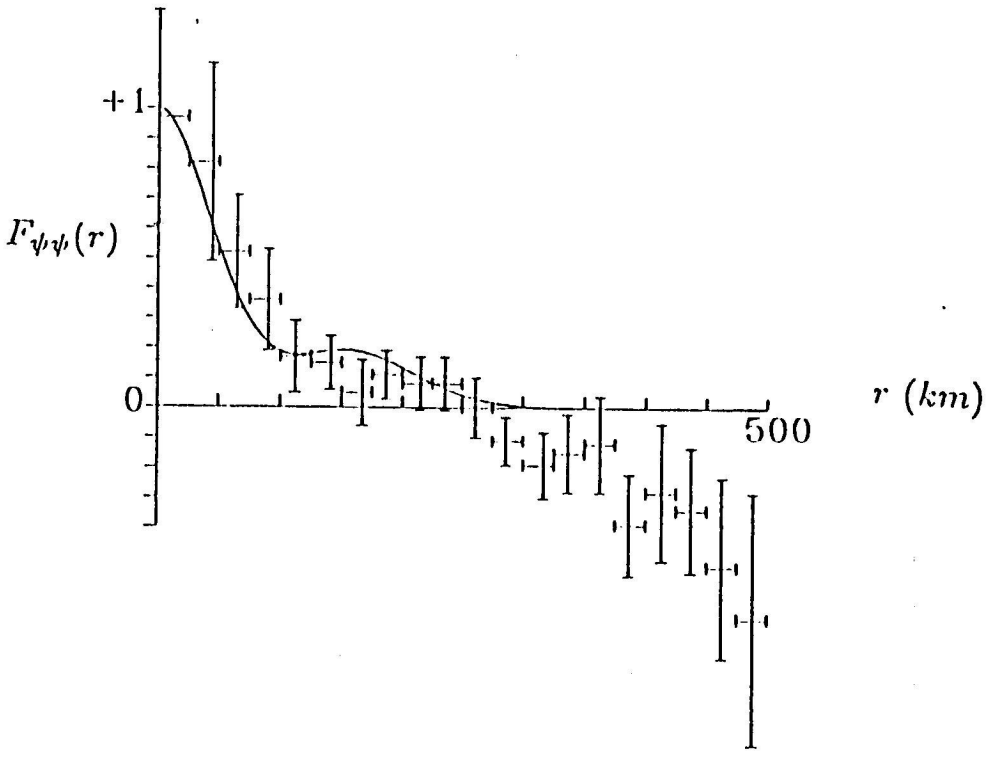

Figure 5.(b) Same as (a) except the three terms of (7a) is used.

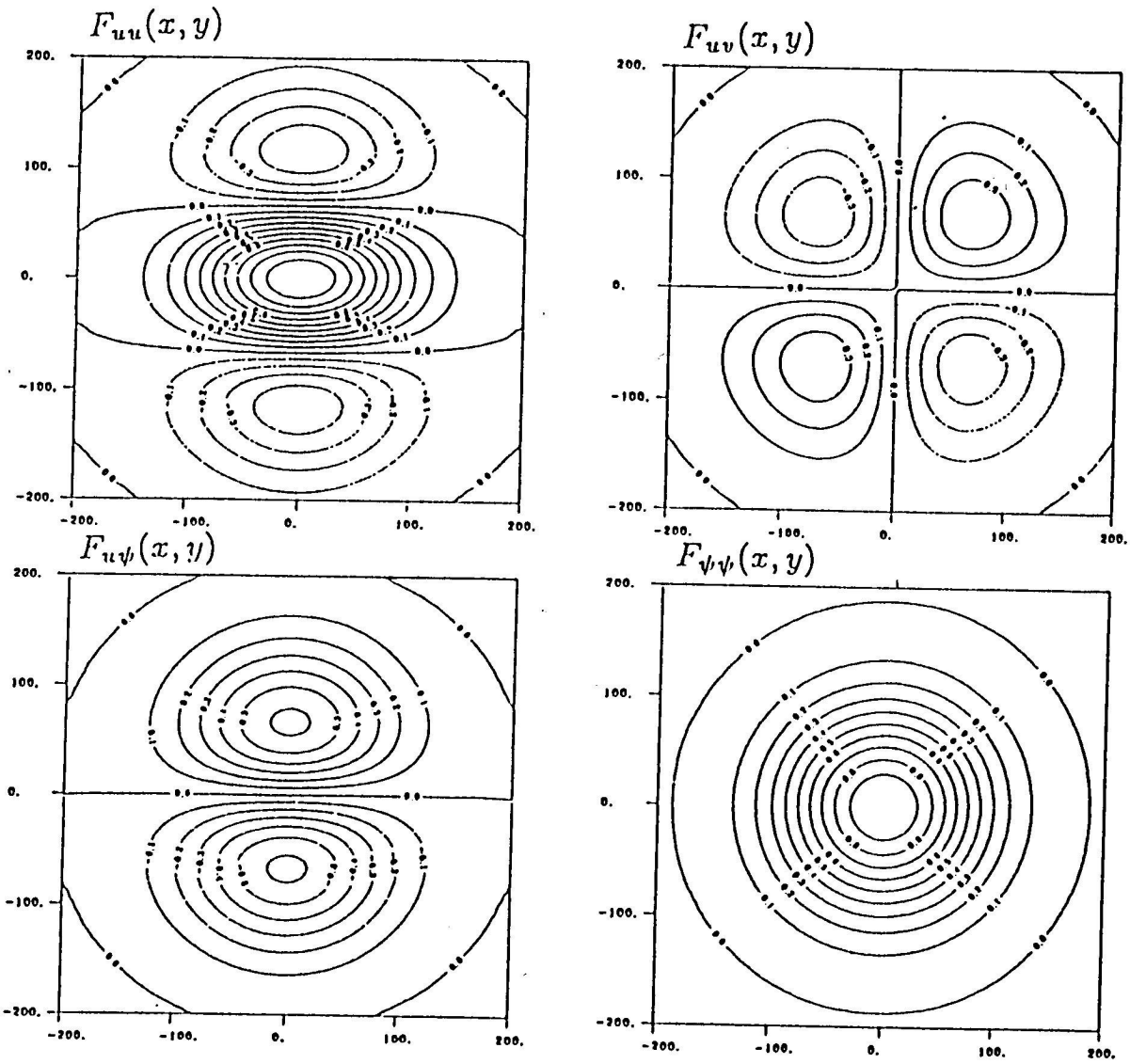

Figure 6.(a) Model correlations for a two term representation of (7a). The axes are x and y separation distances in km.

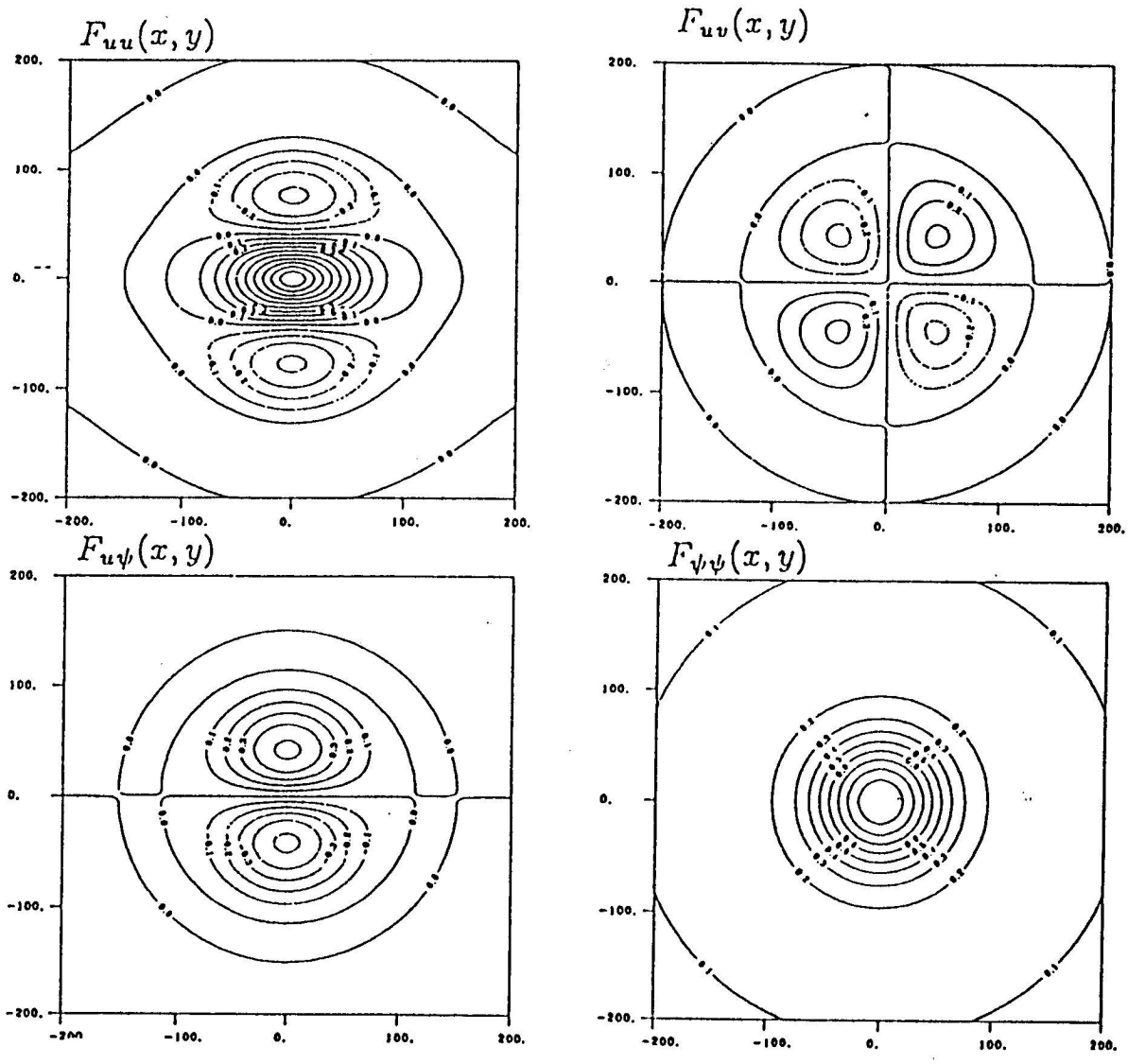

Figure 6.(b) Model correlations for a three term representation of (7a). The axes are x and y separation distances in km.

The extension of the isotropic correlation model, including an arbitrary number of terms in (5) proves to be better than the standard model with the first two terms, as illustrated by comparing two (Figure 5a) and three (Figure 5b) term representations against experimentally determined correlations of dynamical height. The correlation with three terms is relatively narrower than the one with only two terms. The difference between the two fitted functions become more distinct in the case of vector correlations. While the two term model (Figure 6a) is smoother and wider (for the same value of B), the three term correlation model (Figure 6a) has better correspondence with the scales of the observed vector correlations in Figures 4a-f. Because of better agreement with data, we used the three term model in the following analyses.

Analysis with coastal boundary conditions

In bounded ocean domains, the velocity field has to obey coastal boundary conditions. If a sufficient number of observations were available, the information content in the data would impose the physical effects of the boundaries. Because the data is often limited, and because statistical analysis methods do not recognize boundary conditions, the analysed fields do not reflect coastal constraints. In reality, the observations from a coastal circulation would indicate inhomogenous statistics with increasing anisotropy near the coast, as a result of the effects of shelf topography and the coastline geometry. The present-day statistical and numerical models are far removed from a uniform treatment of the open ocean and continental shelf regions.

Basically, the weakness of the analysis to recognize boundaries can be dealt with in two ways: (*i*) the use of inhomogeneous, anisotropic correlation models adapted to boundary conditions, (*ii*) insertion of simulated observations at boundaries consistent with the boundary conditions. In the latter case, if only dynamical height data are used for the analysis, the results depend on a judicious choice of the boundary values; in our earlier studies (Özsoy *et al.*, 1989), we found the method to be unsatisfactory. On the other hand, Robinson *et al.* (1991a) used the equivalent method of specifying synthetic data for temperature and salinity (density) at selected boundaries. Their analyses showed that it was impossible to assign a single boundary value for the entire Eastern Mediterranean coast, so that sources and sinks of flow had to be allowed in some region of the boundary.

A third approach, using the variational inverse method as an alternative to statistical objective analysis is proposed by Brasseur *et al.* (1993). Their methodology also does not recognize coastal boundary conditions but because of smoothness and advection

constraints, seems to produce results approaching (*i*) above, limiting the influence of data points to the region inside the physical ocean domain.

In our analyses, we choose to insert boundary values as artificial observations. Because we use a multi-variate scheme, we can insert either streamfunction or velocity boundary values, by the following schemes along the boundary: (*i*) the specification of a streamfunction value ψ = constant, (*ii*) the free-slip boundary condition, requiring the normal component of velocity to vanish, $\vec{u} \cdot \hat{n} = 0$, or (*iii*) the no-slip boundary condition, in which $(u, v) = 0$.

Note that the boundary value specifications (*i*) and (*ii*) are equivalent according to (6), though the implementation of the second method is less subjective. The first method requires *a priori* knowledge of the constant value to be specified, and a particular choice of the constant value can modify the basin circulation. In the second method, the available observations are interpolated to produce a velocity field along the boundary, setting the normal components to zero; the resulting velocity field is then used as boundary data. In the third method, we give zero velocity components as data along the boundary. The method also allows mixed boundary conditions, with the possibility of assigning a streamfunction value simultaneously with either no-slip or free-slip velocity boundary conditions.

RESULTS

In producing estimates of the streamfunction field, we made simultaneous use of the available CTD and ADCP observations. However, it soon became clear that the choice of analysis parameters and the distribution of the mixed data determined the quality of the analysis. A number of experiments were carried out to observe the individual effects of the available sets of observations, and of the analysis parameters. The measurement standard error variance was taken as $E = 0.1$ for all observations, and the correlation functions corresponding to Figure 6b were used in the analyses. The radius of influence around each analysis point was taken on the order of 120 km and the number of observation points entering an analysis were limited to about 15 for each type of data.

The near-surface (20 m depth) ADCP current measurements in Figure 3c were analysed to yield a streamfunction from u, v data alone, shown in Figure 7a. Comparison with the analysis of dynamical height anomaly in Figure 3a is discouraging; despite a number of trials with different parameters, the field generated by the analysis is noisy,

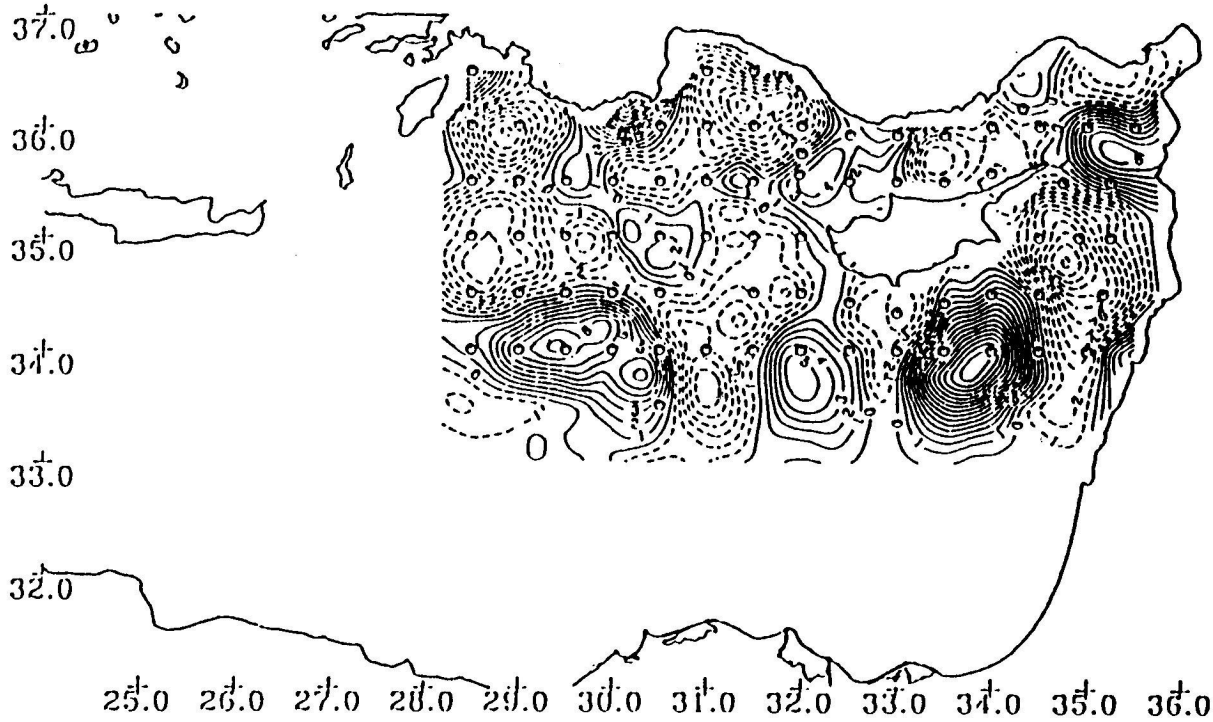

Figure 7.(a) Surface dynamic height anomaly (cm) at 20 m depth, obtained from an analysis of the ADCP cruise-track data of Figure 3.(c),

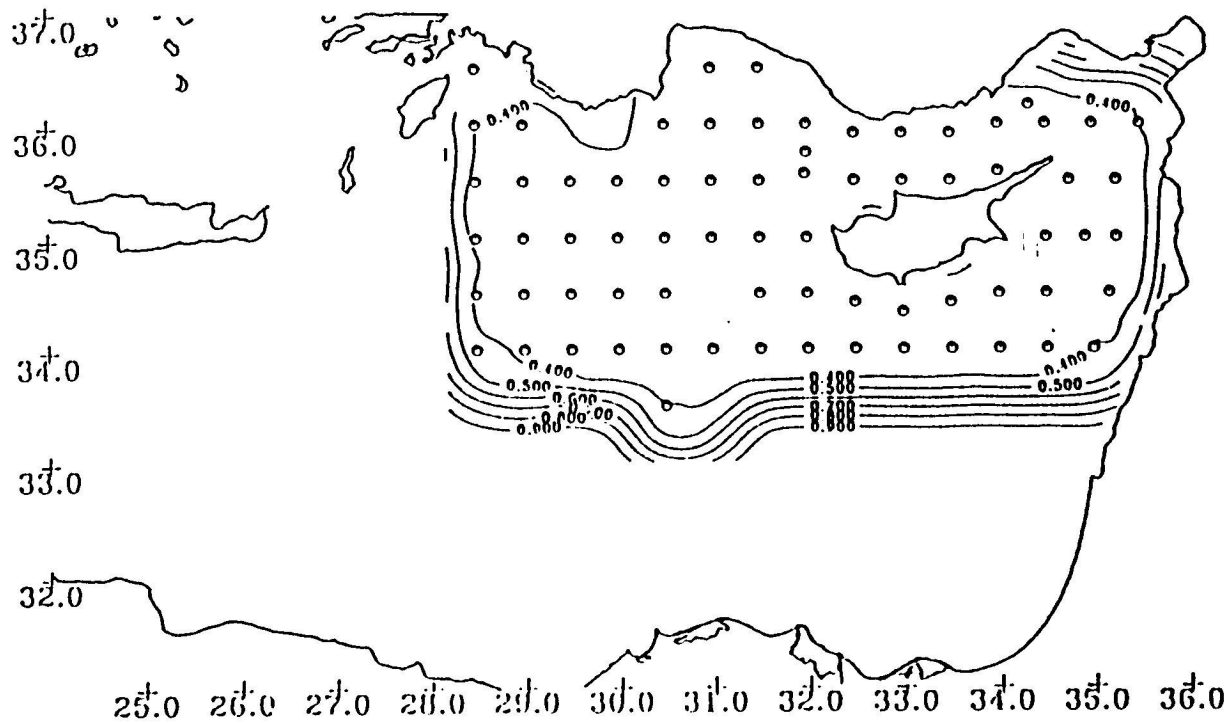

Figure 7.(b) The analysis error variance distribution.

with small scale features embedded in the circulation. We note that the positions of major features and their sense of circulation are consistent with the satellite data of Figure 2 and with the analysis in Figure 3a, despite uncertainties created by the small scales. The generation of small scales appears to be a result of the great number (1133 velocity vectors) of closely spaced observations containing noise. The error variance map in Figure 7b shows that the analysis has an average error variance of 0.4, larger than that specified (0.1) for the observations. This is in agreement with Bretherton *et al.* (1976), who found increased analysis error variance when they used observations spaced at intervals shorter than the horizontal scales of real features. They also showed that further smoothing of noisy observations tended to increase and uniformly distribute the analysis error variance. This result was also confirmed (not shown), because our attempts to smooth the data resulted in further divergence from realistic analysis fields.

As an alternative, we analysed the ADCP current observations obtained at oceanographic stations. The ensemble average currents at 20 m depth, measured every 20 minutes during the ship's stay at each station, are superposed in Figure 8a. The current measurements appear to be stable in direction and magnitude, but considering the relatively short periods in which the currents were measured, the variability may be significant. These measurements were then averaged at each station, and the reference currents at 200 m obtained from the objective analysis of dynamical height data were added to yield the velocity field in Figure 8b.

The analysis of the velocity field in Figure 8b produced the streamfunction field in Figure 9a. The corresponding analysis error variance is shown in Figure 9b. While the circulation essentially includes the same features shown in the satellite data (Figure 2) and the dynamical height analysis of Figure 3a, the location and intensity of these features do not correspond with either set of independent observations. Furthermore, the field generated from the station current measurements is considerably smoother but also different from the analysis of continuous cruise track measurements in Figure 7a, indicating the sensitivity of the analysis to data distribution and quality. Note that the error variance for the analysis of station data (Figure 9b) is slightly higher than the analysis of cruise data (Figure 7b).

Next we analysed the dynamical height anomaly data together with the current velocity. In these test cases we also include different types of coastal boundary conditions. Assuming there is no exchange between the shelf regions and the deep ocean, we apply the coastal boundary condition along the 200 m depth contour, smoothed to eliminate sharp curvatures.

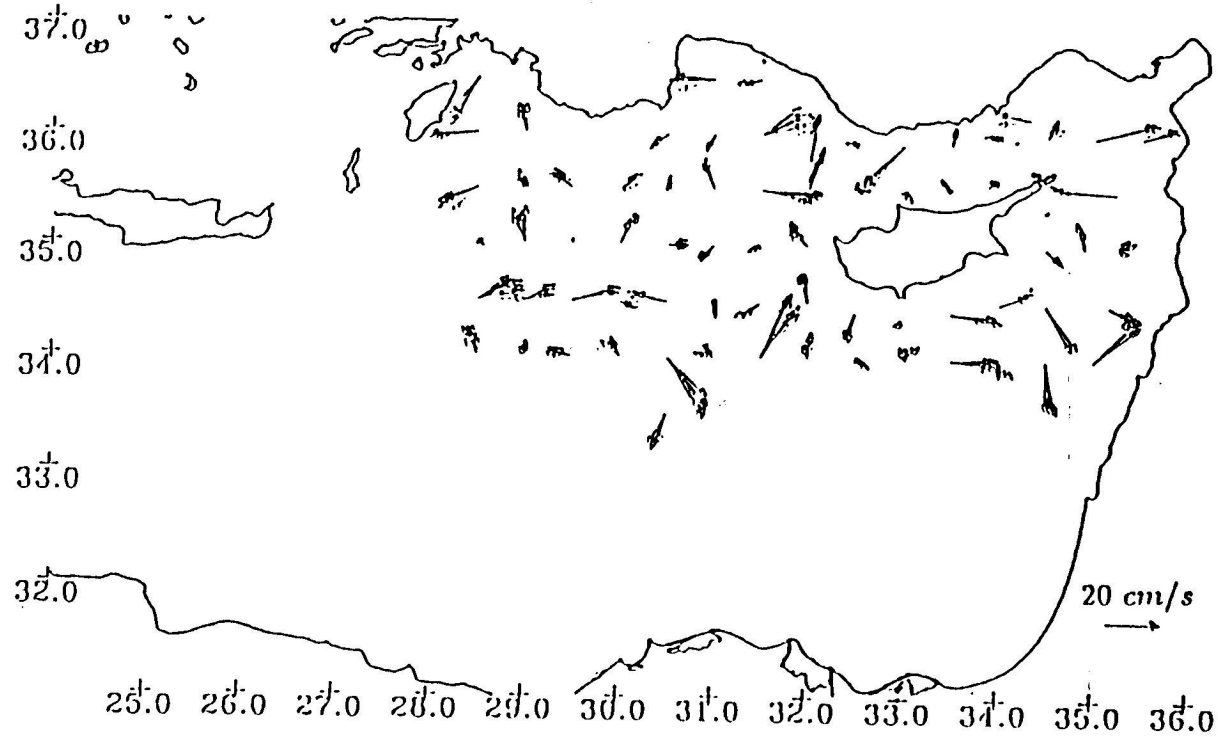

Figure 8.(a) Surface (20 m) current vectors obtained by 30 min ensemble averaging at oceanographic stations.

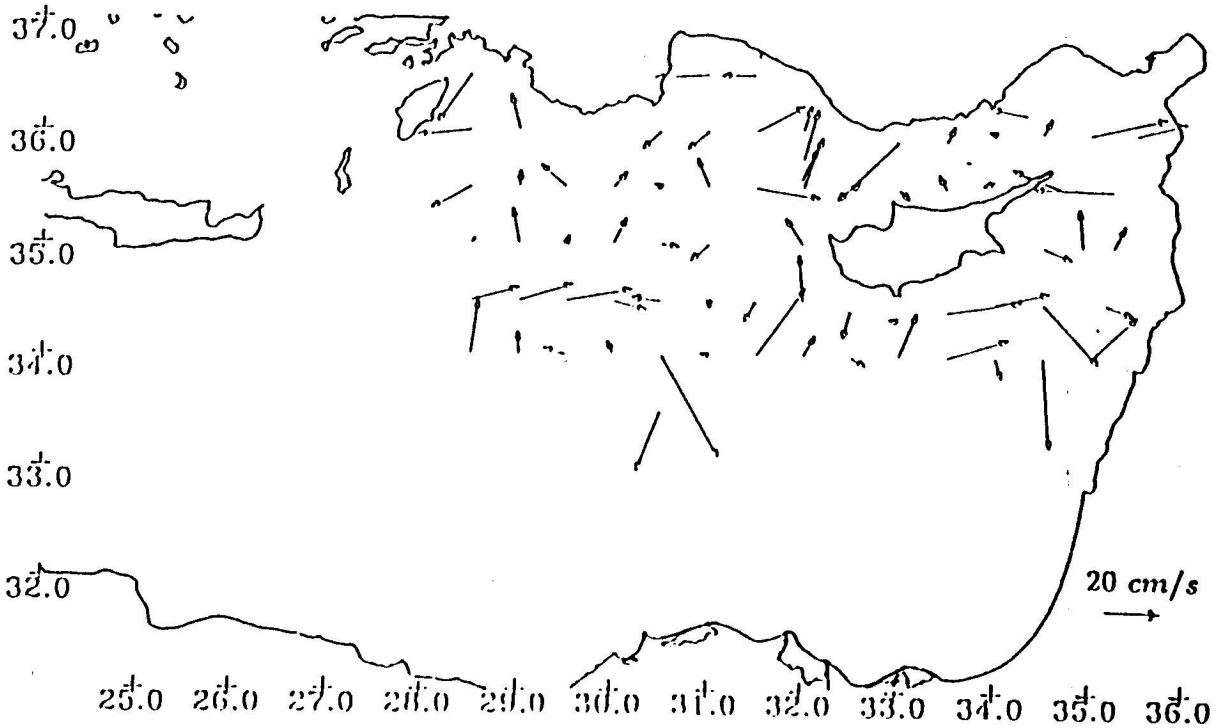

Figure 8.(b) Surface (20 m) current vectors obtained by adding the dynamic height anomaly derived velocity to the averages of (a).

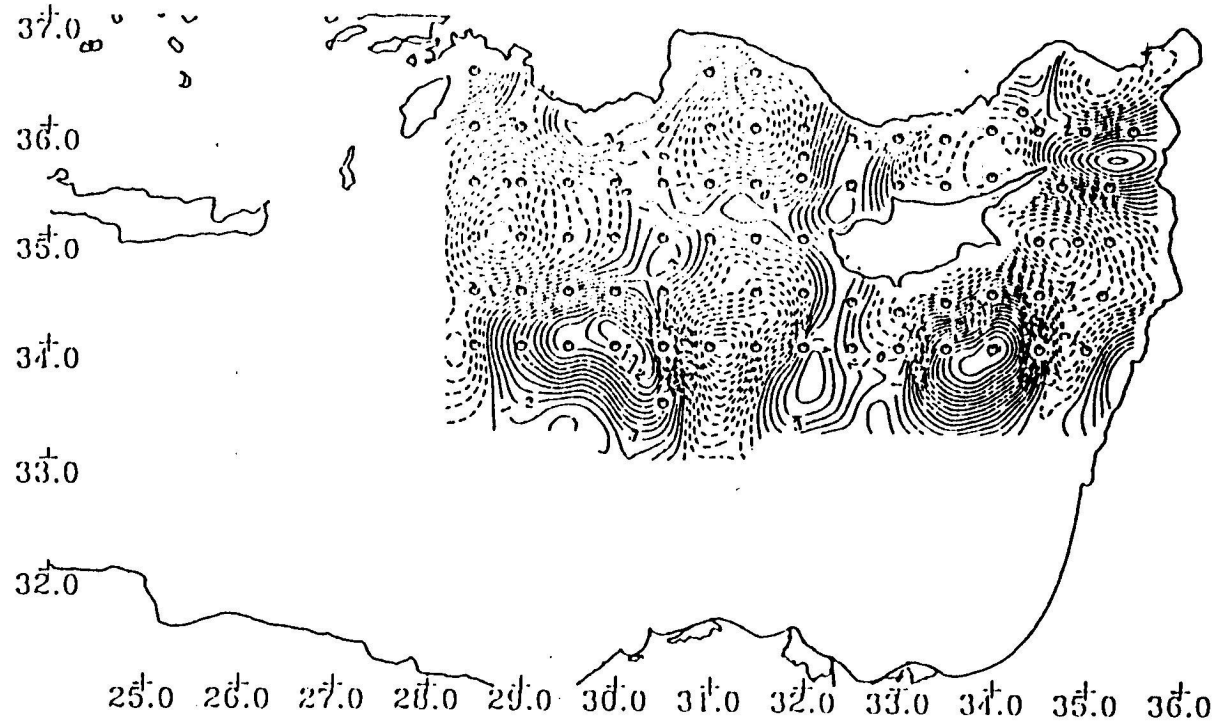

Figure 9.(a) Surface dynamic height anomaly (cm) at 20 m depth, obtained from an analysis of the station ADCP data of Figure 8.(b),

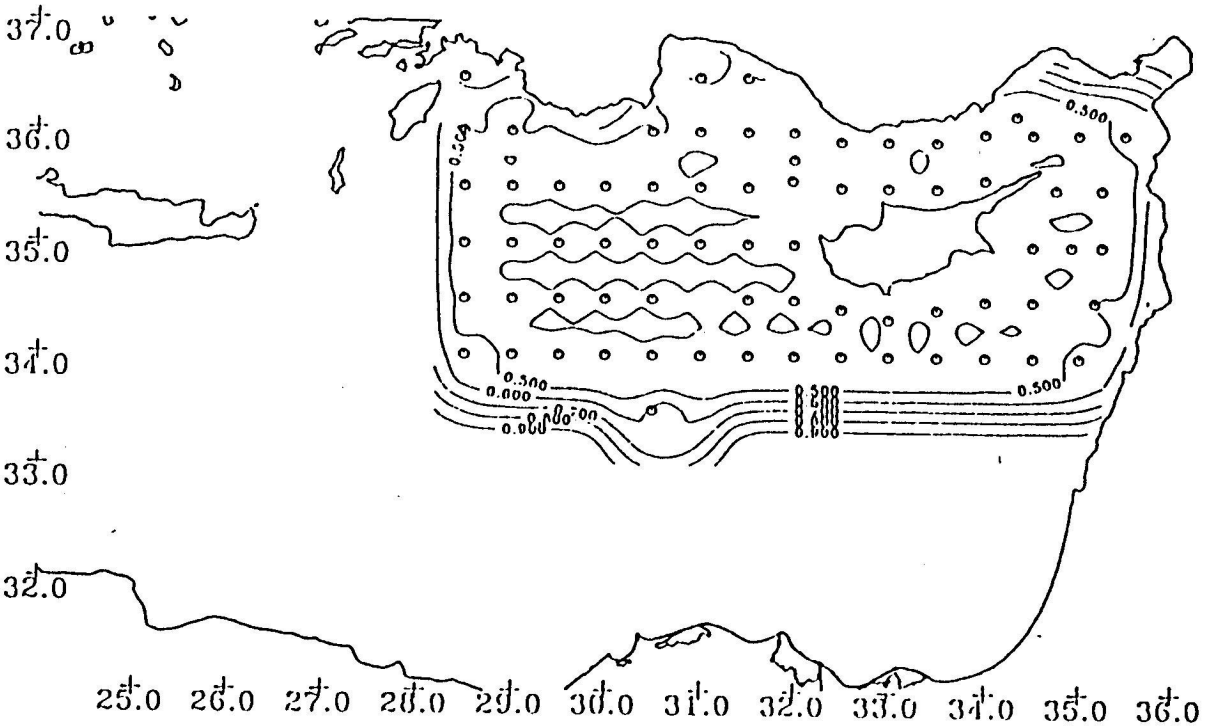

Figure 9.(b) The analysis error variance distribution.

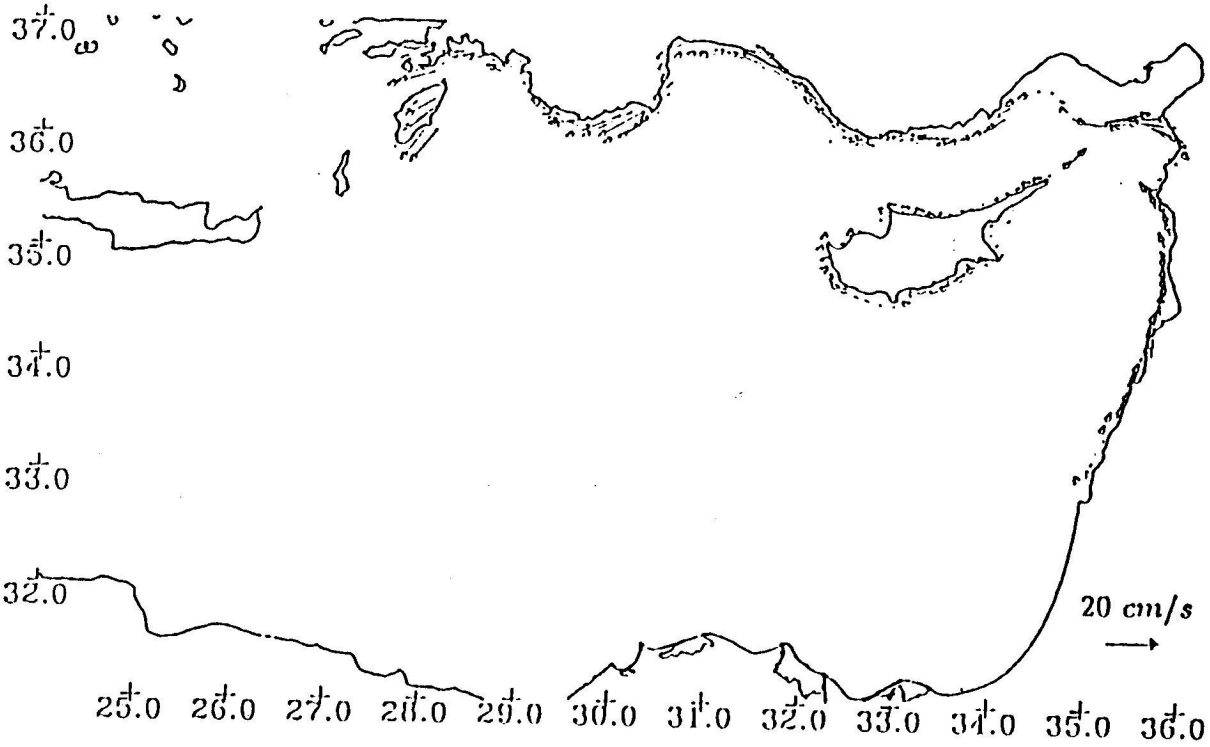

Figure 10 Boundary parallel current velocity vectors generated by projection of interior data on the 200 m depth contour, and keeping the tangential components.

In the no-slip case, we assign zero velocity data along this contour. In the case of the free-slip boundary condition, we project the cruise-track ADCP velocity observations on the boundary by objective analysis, and set equal to zero the components normal to the boundary. The resulting tangential velocity estimates along the 200 *m* depth contour are shown in Figure 10.

The combined analysis of the ψ and (u, v) data at oceanographic stations, with a free-slip boundary condition applied by inserting the boundary velocity data of Figure 10 yields the streamfunction field of Figure 11a. The coastal part of the circulation agrees well with the presence of boundaries. The analysis with a no-slip boundary condition results in a slightly different field (Figure 11b), especially near the coasts where the requirement to have vanishing tangential velocity (*i.e.* a vanishing normal gradient of ψ), forces the maximum currents of the jet flows to be moved away from coastal boundaries.

The analysis of combined interior data together with combined boundary values seems to work best. The boundary conditions can include the constant streamfunction

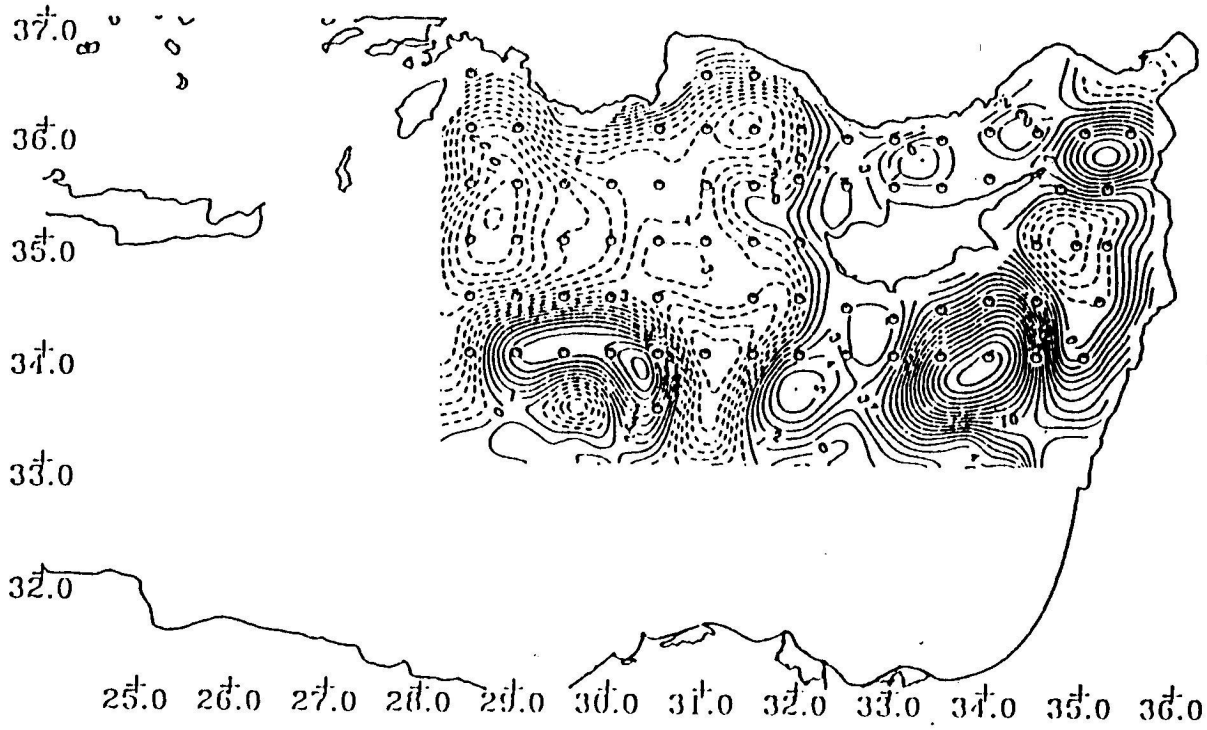

Figure 11.(a) Surface dynamic height anomaly (cm) at 20 m depth, obtained from a combined analysis of the station CTD and ADCP data, and the tangential velocity data of Figure 10.(b) applied at the boundary (free-slip boundary condition).

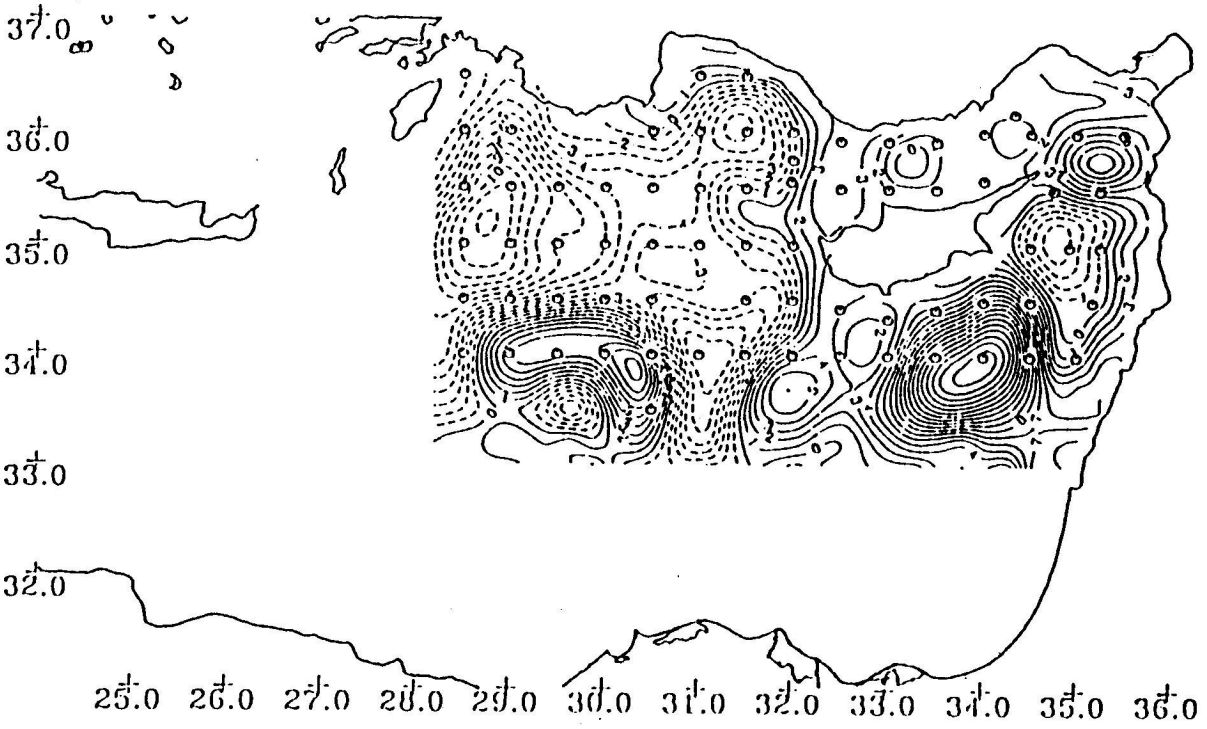

Figure 11.(b) Same as (a) except that the boundary velocity components are set equal to zero (no-slip boundary condition).

assignment, either with free-slip or no-slip velocity boundaries, as long as the boundary streamfunction is objectively determined. These mixed boundary data reinforce each other in Figure 12a, and the difference from Figure 11a is only minimal. A constant value of $\psi = 3\ cm$ was used along the mainland coasts and on the coast of Cyprus, determined first with a projection of streamfunction values by objective analysis, and averaging along each coast. The island and basin boundary values were equal in this case of October 1991 observations, because the jet proceeding west of Cyprus joins the Anatolian coast without branching to the east, though we note that this need not be the case for other realizations of the circulation (*e.g.* Özsoy *et al.*, 1993).

Finally, note that the analysis error variance is reduced to less than 0.1 in the combined analysis (Figure 12b). This result shows that the dynamical height observations compensate for the analysis errors of the relatively more noisy current velocity observations. Note, however, that both sets of independent observations have comparable weights in determining the circulation, since the circulation in Figure 12a has better defined eddies, jets and meanders whose features derive from the independent analyses of Figures 3a and 7a. Yet, the multi-variate technique appears to the be best way to incorporate the effects of each measurement into the analyis, yielding estimates better than those produced from the individual sets of data. This is evident in Figure 12a, which seems consistent with basic features in Figure 2, including additional detail not presented by Figure 3a.

The stratification characterizing the survey period is displayed in Figure 13a. The first three baroclinic quasi-geostrophic dynamical modes, computed for this N^2 profile, with an average depth of 2400 m assumed for the Levantine Basin, are shown in Figure 13b. Note that the dynamical modes are trapped near the surface (within the first 500 m). The corresponding Rossby radii are 12.1, 6.4 and 3.8 km respectively. The vertical dependence of the coastal values of the boundary streamfunction determined by our analysis scheme compared well with the first baroclinic eigenmode at model levels. We will report on the model results in a forthcoming publication.

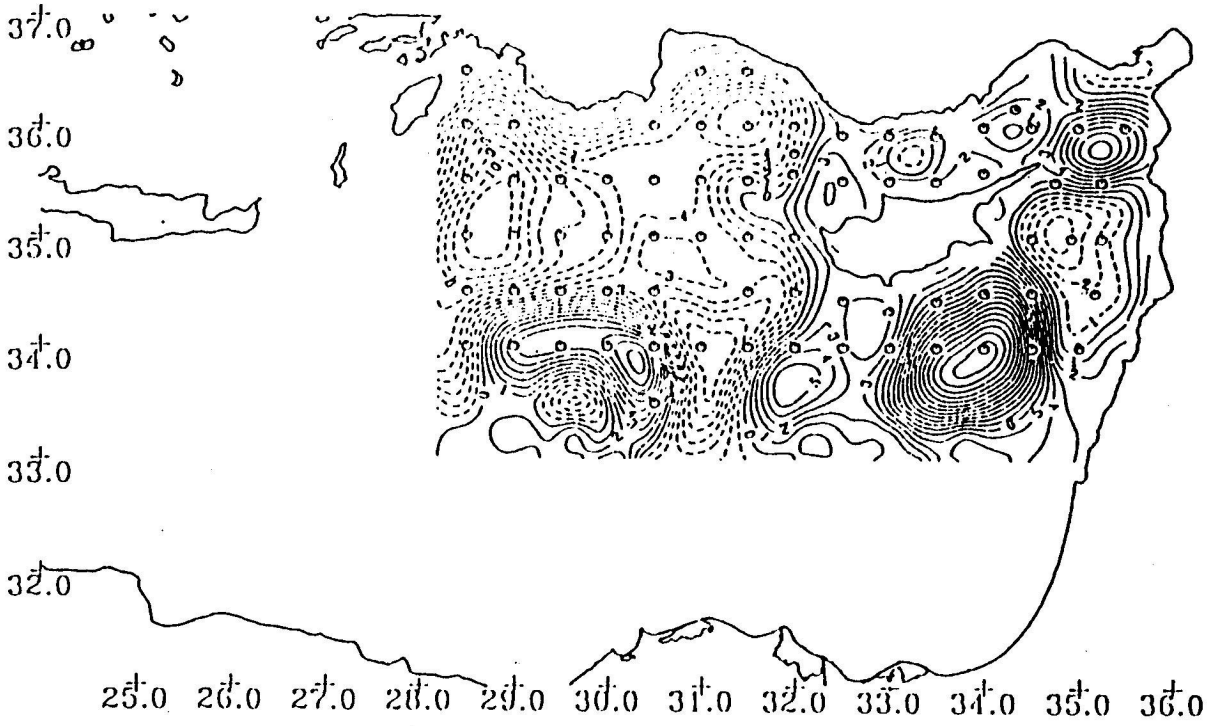

Figure 12.(a) Surface dynamic height anomaly (cm) at 20 m depth, obtained from a combined analysis of the station CTD and ADCP data, and the tangential velocity data of Figure 10,

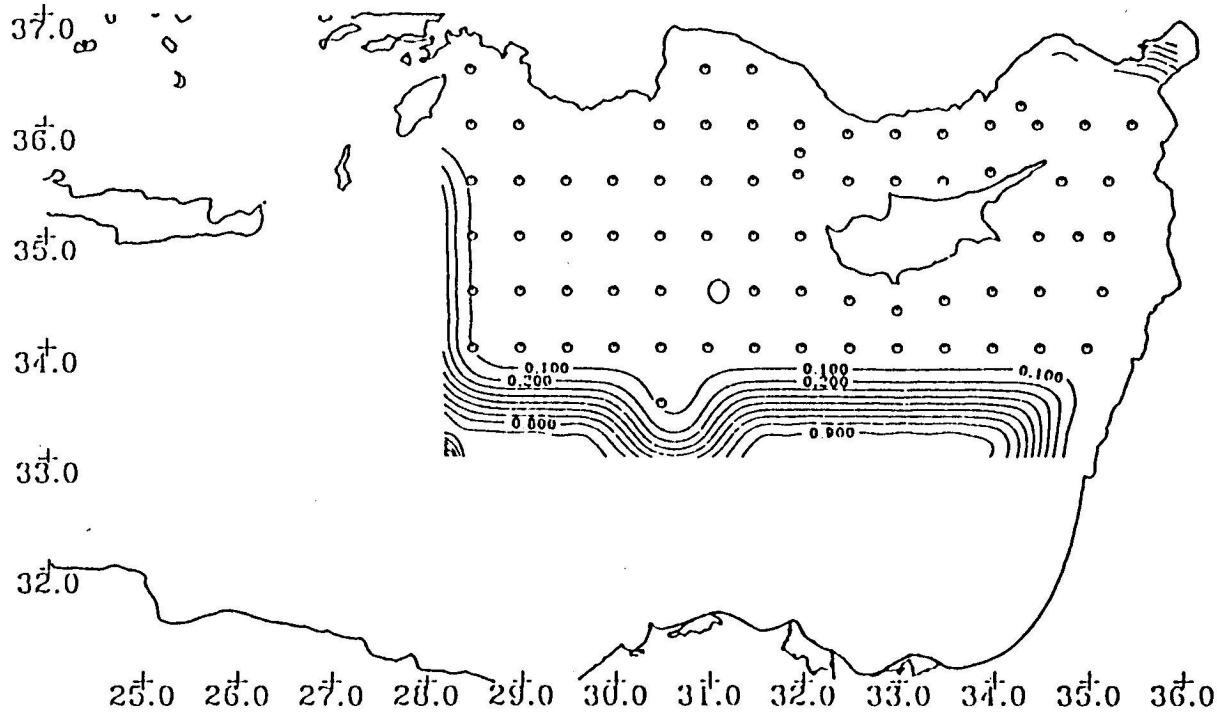

Figure 12.(b) The analysis error variance distribution.

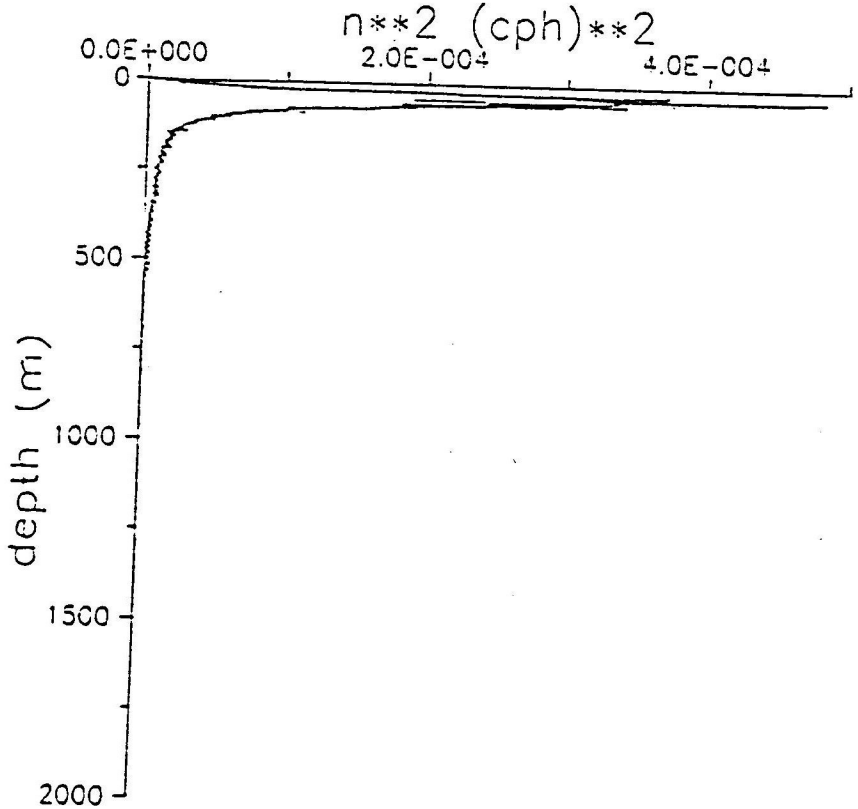

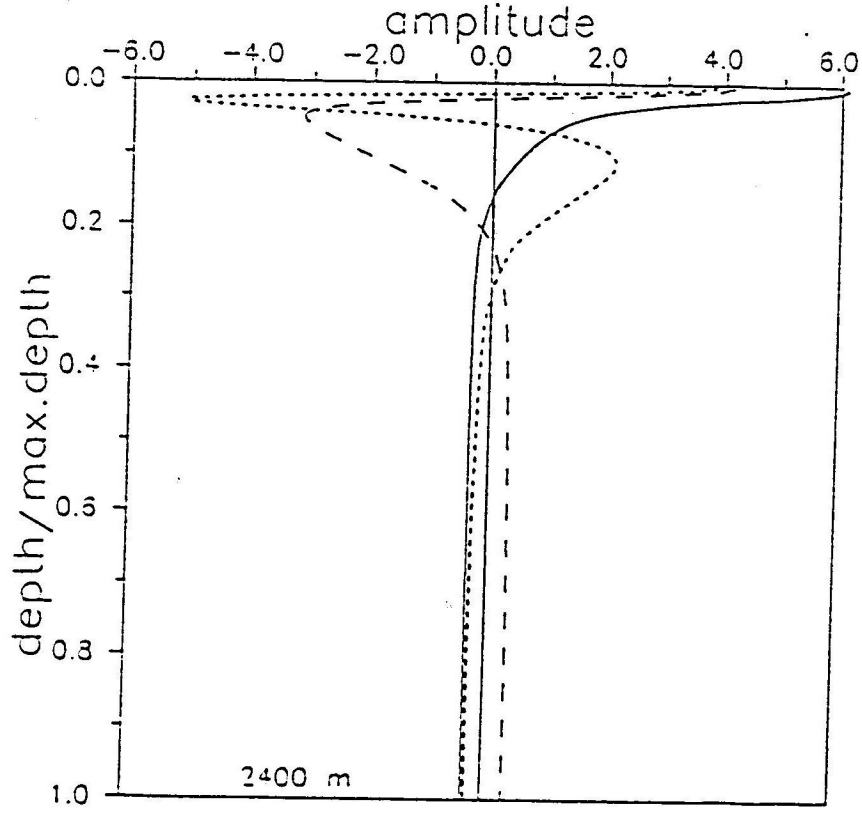

Figure 13.(a) Vertical profile of the stratification parameter $N^2 = -\frac{g}{\rho}\frac{d\rho}{dz}$ *obtained from an average of the CTD data, October 1991, (b) The first three baroclinic dynamical modes of the quasigeostrophic vertical structure equation for the* N^2 *profile in (a).*

CONCLUSIONS

The dilemma of making maximum use of quasi-synoptic, three-dimensional, yet imperfect observational data, and extracting the information content compatible with physical laws, is a modern problem of ocean science. Advances in this field are being made by developing elaborate methods for assimilating data into models.

The Levantine Basin is a region of coherent ocean structures with complex interactions. Modelling would gain from improved estimates of initial fields. Our experience shows that the best synthesis of the observations in this environment is done by combined analysis of the available data, and by applying constraints to satisfy approximate coastal boundary conditions.

Our attempts to use the continuous measurements of current velocity collected at cruise time did not produce sufficiently reliable results. This may be due to the noise content of the observations, their distribution and weaknesses of the analysis method. The effect of a single observation on the analysis field is proportional to the correlation functions shown in Figures 5a,b. For example, the streamfunction contribution of each velocity observation is proportional to the $F_{u\psi}$, with an influence function in the form of a dipole. Superposition of many dipoles creates a noisy field unless there is perfect correspondence between the observations and the model correlation. We believe better results can be obtained with further improvements in the statistical model.

REFERENCES

Bergamasco, A., Malanotte-Rizzoli, P., Thacker, W. C., and R. B. Long, 1993. The Seasonal Steady Circulation of the Eastern Mediterranean Determined with the Adjoint Method, *Deep-Sea Res.*, (in press).

Bergamasco, A., 1993. Data Assimilation Using the Adjoint Method: Problems and New Perspectives, presented at the 25^th International Liège Colloquium on Ocean Hydrodynamics, Liège, May 3-7, 1993.

Brasseur, P., Brankart, J.-M., Beckers, J.-M., Haus, J. and J. Nihoul, 1993. Reconstruction of Oceanic Data Fields and Data Assimilation, presented at the 25^th International Liège Colloquium on Ocean Hydrodynamics, Liège, May 3-7, 1993.

Bretherton, F. P., Davis, R. E. and C. B. Fandry, 1976. A Technique for Objective Analysis and Design of Oceanographic Experiments Applied to Mode-73, *Deep-Sea Res*, 23, 559 - 582.

Brenner, S., Rozentraub, Z., Bishop, J. and M. Krom, 1991. The Mixed Layer / Thermocline Cycle of a Persistent Warm Core Eddy in the Eastern Mediterranean. *Dyn. Atmos. Oceans*, 15, 455-476.

Feliks, Y., 1991. Downwelling along the Northern Coast of the Eastern Mediterrranean, *J. Phys. Oceanogr.*, 21, 511-526.

Feliks, Y. and M. Ghil, 1993. Downwelling-Front Instability and Eddy Formation in the Eastern Mediterranean, *J. Phys. Oceanogr.*, 23, 61-78.

Denman K. L. and H. J. Freeland, 1985. Correlation Scales, Objective Mapping and a Statistical Test of Geostrophy over the Continental Shelf, *J. Mar. Res.*, 43, 517 - 539.

Lascaratos, A., Williams, R. G. and E. Tragou, (1993). A Mixed - Layer Study of the Formation of Levantine Intermediate Water, (submitted for publication).

Malanotte-Rizzoli, P. and A. Bergamasco, 1989. The General Circulation of the Eastern Mediterranean, Part I: The Barotropic, Wind-Driven Circulation, *Oceanol. Acta*, 12, 335-351.

Malanotte-Rizzoli, P. and A. Bergamasco, 1991. The Wind and Thermally Driven Circulation of the Eastern Mediterranean Sea. Part II: The Baroclinic Case, *Dyn. Atmos. Oceans*, 15, 355-419.

McWilliams, J. C., Owens, W. B., and B. L. Hua, 1986. An Objective Analysis of the POLYMODE Local Dynamics Experiment. Part I: General Formalism and Statistical Analysis, *J. Phys. Oceanogr.*, 16, 483 - 504.

Ovchinnikov, I. M. and A. Plakhin, 1984. The Formation of Intermediate Waters of the Mediterranean Sea in the Rhodes Cyclonic Gyre, *Oceanology*, 24, 317-319.

Özsoy, E., Hecht, A. and Ü. Ünlüata, 1989. Circulation and Hydrography of the Levantine Basin, Results of POEM Coordinated Experiments 1985/1986, *Prog. Oceanogr.*, 22, 125-170.

Özsoy, E., Hecht, A., Ünlüata, Ü., Brenner, S., Oğuz, T., Bishop, J., Latif, M. A., Z. Rozentraub, 1991. A Review of the Levantine Basin Circulation and its Variability during 1985-1988, *Dyn. Atmos. Oceans*, 15, 421-456.

Özsoy, E., Lozano, C. and A. R. Robinson, 1992. A Baroclinic Quasigeostrophic Model for Closed Basins or Semi-Enclosed Seas with Islands, *Mathematics and Computers in Simulations*, 34, 51-79.

Özsoy, E. and Ü. Ünlüata, 1992. Dynamical Aspects of the Cilician Basin, Northeastern Mediterranean, in: *Winds and Currents of the Mediterranean Basin, Volume II* (proceedings of a NATO ASI at Santa Teresa, La Spezia, Italy, 1983), Charnock, H.,

editor, Reports in Meteorology and Oceanography, The Division of Applied Sciences, Harvard University, 40 and 41, 1-34.

Özsoy, E. and Ü. Ünlüata, 1993. *Physical Oceanography of the Eastern Mediterranean*, In: *Mediterranean Seas 2000*, N. F. R. Della Croce, editor, University of Genoa 489 pp. (Proceedings of the 'Mediterranean Seas 2000' Symposium, University of Genoa, Santa Margherita Ligure, Italy, 23-27 September 1991)

Özsoy, E., Hecht, A., Ünlüata, Ü., Brenner, S., Sur, H. İ., Bishop, J., Latif, M. A., Rozentraub,Z. and T. Oğuz, 1993. A Synthesis of the Levantine Basin Circulation and Hydrography, 1985-1990, *Deep-Sea Res*, (in press).

Pinardi, N. and A. Navarra, 1992. Baroclinic Wind Adjustment Processes in the Mediterranean Sea, *Deep-Sea Research*, (in press).

The POEM Group (Robinson, A. R., Malanotte-Rizzoli, P., Hecht, A., Michelato, A., Roether, W., Theocharis, A., Ünlüata, Ü., Pinardi, N., Artegiani, A., Bishop, J., Brenner, S., Christianidis, S., Gacic, M., Georgopoulos, D., Golnaraghi, M., Hausmann, M., Junghaus, H.-G., Lascaratos, A., Latif, M. A., Leslie, W. G., Oğuz, T., Özsoy, E., Papageorgiou, E., Paschini, E., Rosentroub, Z., Sansone, E., Scarazzato, P., Schlitzer, R., Spezie, G.-C., Zodiatis, G., Athanassiadou, L., Gerges, M., Osman, M.), 1992. General Circulation of the Eastern Mediterranean, *Earth Science Reviews*, 32, 285-309.

Robinson, A. R. and W. G. Leslie, 1985. Estimation and Prediction of Oceanic Eddy Fields, *Progr. Oceanogr.*, 14, 485-510.

Robinson, A. R. and E. F. Carter, 1987. Analysis Models for the Estimation of Oceanic Fields, *J. Atmos. Oceanic Technol.*, 4, 49-74.

Robinson, A. R., Golnaraghi, M., Leslie, W. G., Artegiani, A., Hecht, A., Michelato, A., Sansone, E., Theocharis, A. and Ü. Ünlüata, 1991a. The Eastern Mediterranean General Circulation: Features, Structure and Variability, *Dyn. Atmos. Oceans*, 15, 215-240.

Robinson, A. R., Golnaraghi, M., Lozano, C. J., Milliff, R. and E. Özsoy, 1991b. Data Assimilation in Quasigeostrophic Model with Arbitrary Coasts and Islands, 23 rd International Liège Colloqium on Ocean Hydrodynamics, Modelling the Interaction of the Deep Ocean and the Shelf and Coastal Seas, Liège, 6-10 May 1991.

Robinson, A. R. and M. Golnaraghi, 1992. Circulation and Dynamics of the Eastern Mediterranean Sea; Quasi-Synoptic Data-Driven Simulations (submitted for publication).

Roussenov, V. and P. P. Brasseur, 1992. A Comparative Analysis of Climatological Fields in the Mediterranean Sea, Presses Universitaires de Liège, Liège, Belgium.

Roussenov, V., Stanev, E., Artale, V., and N. Pinardi, 1993. A Seasonal Model of the Mediterranean Sea General Circulation, (submitted for publication).

Saunders, P. M., 1992. Combining Hydrographic and Shipborne ADCP Measurements, *Deep-Sea Res.*, 39, 1417-1427.

Sur, H. İ., Özsoy, E., and Ü. Ünlüata, 1992. Simultaneous Deep and Intermediate Depth Convection in the Northern Levantine Sea, Winter 1992, *Oceanologica Acta, in press.*

Tziperman, E., and P. Malanotte-Rizzoli, 1991. The Climatological Seasonal Circulation of the Mediterranean Sea, *J. Mar. Res.*, 49, 411-434.

Walstad, L. J., Allen, J. S., Kosro, P. M., and A. Huyer, 1991. Dynamics of the Coastal Transition Zone Through Data Assimilation Studies, *J. Geophys. Res.*, 96, 14959-14977.

Zavatarelli, M. and G. L. Mellor, 1993. A Numerical Study of the Mediterranean Sea Circulation, *J. Phys. Oceanogr.*, (in press)